Discrete layers of interacting growing protein seeds: Convective and morphological stages of evolution

Marcello Lappa*
MARS (Microgravity Advanced Research and Support Center), Via Gianturco 31-80146, Napoli, Italy
(Received 22 July 2004; revised manuscript received 20 December 2004; published 15 March 2005)

The growth of several macromolecular seeds uniformly distributed on the bottom of a protein reactor (i.e., a discrete layer of N crystals embedded within a horizontal layer of liquid with no-slip boundaries) under microgravity conditions is investigated for different values of N and for two values of the geometrical aspect ratio of the container. The fluid dynamics of the growth reactor and the morphological (shape-change) evolution of the crystals are analyzed by means of a recently developed moving boundary method based on differential equations coming from the protein "surface incorporation kinetics." The face growth rates are found to depend on the complex multicellular structure of the convective field and on associated "pluming phenomena." This correspondence is indirect evidence of the fact that mass transport in the bulk and surface attachment kinetics are competitive as rate-limiting steps for growth. Significant adjustments in the roll pattern take place as time passes. The convective field undergoes an interesting sequence of transitions to different values of the mode and to different numbers of rising solutal jets. The structure of the velocity field and the solutal effects, in turn, exhibit sensitivity to the number of interacting crystals if this number is small. In the opposite case, a certain degree of periodicity can be highlighted for a core zone not affected by edge effects. The results with no-slip lateral walls are compared with those for periodic boundary conditions to assess the role played by geometrical constraints in determining edge effects and the wavelength selection process. The numerical method provides "microscopic" and "morphological" details as well as general rules and trends about the macroscopic evolution (i.e., "ensemble behaviors") of the system.

DOI: 10.1103/PhysRevE.71.031904 PACS number(s): 87.15.Nn, 81.10.Dn, 47.20.Hw, 02.70.−c

I. INTRODUCTION

Proteins are the elementary building units of all living creatures and essential components for information and energy processing within living systems.

The crystallization process of these substances has been the focus of intense investigation for many decades, and recently a tremendous effort has been devoted to the study of these topics. Progress in various biochemical and biomedical research and production tasks in fact is still impeded by a lack of insight into the growth mechanisms of these complex molecules that are very labile and sensitive to the conditions under which they are operated (see the excellent book of Vekilov and Chernov [1] and McPherson [2]). It is worthwhile to point out also how, in addition to its medical and biotechnological significance, protein crystallization exhibits a theoretical kinship with the complex of problems that come under the heading "order out of chaos." Protein crystallization can be seen in fact as a good terrain for testing our current ability to predict the behavior of complex systems (fundamental research, nonlinear behaviors, etc.).

Since the production of protein crystals of adequate size and desired quality is often the bottleneck of the available techniques, today the major effort is devoted to a better understanding of the conditions that may influence their growth. Such knowledge may support the introduction of new crystallization techniques and the design of new reactors.

Since it is expected that growth is driven by the phenomena occurring in a thin zone surrounding the crystal (the so-called "depletion zone;" see, e.g., [3,4]) where the concentration of the nutrients is lowered due to solute absorption, many authors have focused on "what happens close to the crystal."

The procedure usually employed in these studies consists in growing a very limited number (N) of "seeds" (see, for instance, the excellent works of Otálora *et al.* [4,5], Lee and Chernov [6], etc.). In practice, multiple-nucleation events are obtained in gel [$N=O(100)$] usually by a counter diffusion technique (for further details about this technique and its models see, e.g., Refs. [7–11]); then, the nuclei are grown in this environment up to a desired size (this growth technique is known to produce "reinforced" crystals that can be easily handled and can even be glued to rigid substrates, Otálora *et al.* [4]). At this stage some crystals with large size (not many) are placed in a new (small) reactor expressly conceived and equipped for surface analysis (*in situ*, nonintrusive monitoring techniques). At this stage they are called "seeds." Particular care is devoted to avoid further nucleation phenomena (i.e., the formation of new nuclei) that would spoil interferometry data.

Often gel is not used for this second stage of growth since it is well known that it can have detrimental effects on the final quality of the specimens. Usually, in fact, these experiments are carried out taking advantage of microgravity conditions (in order to benefit of the quiescent or quasiquiescent conditions that are established in this environment).

Microgravity has the advantage over gels of being free of macromolecular interactions that could modify in unex-

*Electronic address: marlappa@marscenter.it, marlappa@unina.it

pected ways the surface kinetics. Unfortunately, however, often convection arises due to residual gravity disturbances and the growth process can be associated with the onset of morphological instabilities driven by these convective effects (i.e., shape change of the growing specimens). The understanding of these phenomena is crucial in determining generalized criteria to obtain well-controlled growth (i.e., final samples of desired shape and size).

Along these lines, mathematical and numerical analyses can be regarded as a necessary, additional tool for gaining such a knowledge.

Excellent numerical simulations to elucidate the interaction between organic crystal growth and convection due to solutal buoyancy forces were initially carried out by Lin *et al.* [12] who used a kinetic-coefficient-based differential surface condition and predicted (in principle) possible onset of surface depressions and/or protuberances in terms of growth rate surface distributions. An interesting contribution dealing with the application of "moving boundary" techniques to the problem of a crystal growing in a supersaturated solution was provided by Noh, Koh, and Kang [13], who obtained numerical solutions through numerically generated orthogonal curvilinear coordinate systems, automatically adjusted to fit the boundary shape at any instant. Several of the many modern numerical methods currently used in the representation of discontinuities (boundaries, fronts and interfaces) moving with a fluid, however, are capable to undertake a fixed-grid solution without resorting to mathematical manipulations and transformations (for a very comprehensive discussion dealing with a historical perspective, the genesis, and the evolution of these methods see, e.g., Rider and Kothe [14], Kim, Goldenfeld, and Dantzig [15] and references therein). These numerical strategies have enjoyed widespread use for the simulation of typical problems dealing with gas/liquid or liquid/liquid systems (where the surface tension effects play a "critical role" in determining the shape of the fluid/fluid interface and/or its motion) as well as with the case of thermal solidification of melts.

Recently these techniques have been extended to the case of macromolecular growth (due to the addition and incorporation of solute molecules (building blocks or growth units) to the crystal lattice) and to the growth of organic "living" tissues in bioreactors [16]. For instance, they were used by Lappa [17] to "track" the evolution of the solid/liquid interface of a single sample surrounded by the nutrient solution, focusing on the surface kinetics and their sensitivity to many "local" environmental factors. A quite exhaustive attempt dealing with the case of two interacting crystals was provided by Lappa [18]. The case of protein seeds sharing the same growth reactor was investigated under the effect of a residual-g (microgravity conditions). It was shown that the size and shape of the growing crystals play a "critical role" in the relative importance of surface effects and in determining the intensity of convection. Convective effects, in turn, were found to impact growth rates, macroscopic structures of precipitates, particle size, and morphology as well as the relative importance of mass transport in liquid phase and surface attachment kinetics. Some interesting scaling models dealing with the importance of convective effects and slow surface kinetics were also provided by Lee and Chernov [6] and Otálora *et al.* [5]. The simulations of Lappa [18] showed in detail that this relative importance does not behave as a "fixed" parameter and that different crystallization conditions may occur in the protein chamber due to mutual interference of the growing seeds, complex convective effects, and "finite size" of the reactor.

In the present paper that preliminary analysis is extended to the case of N crystals, i.e., several protein seeds uniformly distributed on the bottom of a protein reactor (i.e., a discrete layer of N crystals for different values of N). "Ensemble behaviors" with many specimens, in fact, are also an important aspect of the problem. For $N \gg 1$, in fact, crystallization at a macroscopic scale is characterized by the interplay of different phenomena: transport in liquid phase, convection, and in particular competition among different crystals.

Due to their geometric complexity, such configurations have not been studied in great detail. They are still a challenging task for numerical simulation. The present contribution appears as the first attempt to analyze these (fluid-dynamic) global behaviors focusing on both microphysical and macrophysical aspects. The analysis is carried out through application of the kinetic model used by Lappa [16,17] (able to take into account convective effects, and to model all those factors dealing with the "local" history of the crystal shape). It is briefly described in the next section.

II. MATHEMATICAL MODEL AND NUMERICAL METHOD

A. OCGVOF method: General properties

This method accounts for the solid mass stored in the generic computational cell by assigning an appropriate value of ϕ (phase field variable) to each mesh point ($\phi=1$ crystal, $\phi=0$ feeding solution, and $0<\phi<1$ for an interfacial cell).

In the presence of convection, the flow is governed by the continuity, Navier-Stokes, and species equations, which in nondimensional conservative form read

$$\nabla \cdot \mathbf{V} = 0, \tag{1}$$

$$\frac{\partial \mathbf{V}}{\partial t} = -\nabla p - \nabla \cdot [\mathbf{V}\mathbf{V}] + \mathrm{Sc}\nabla^2 \mathbf{V} + \mathrm{ScRa}\left(\frac{C}{C_{(0)}} - 1\right)\hat{\mathbf{i}}_g + \frac{D_{salt}}{D}\mathrm{ScRa}_{salt}\left(\frac{C_{salt}}{C_{salt(0)}} - 1\right)\hat{\mathbf{i}}_g - \mathrm{Sc}\frac{1}{\eta}\mathbf{V}, \tag{2}$$

where ν is the kinematic viscosity, D is the protein diffusion coefficient, $\mathrm{Sc}=\nu/D$, $\mathrm{Ra}=g\beta_{prot}C_{(0)}L^3/\nu D$, and $\mathrm{Ra}_{salt}=g\beta_{salt}C_{salt(0)}L^3/\nu D_{salt}$ (the Boussinesque approximation is used to model the buoyancy forces, and β_{prot} and β_{salt} are the solutal expansion coefficients related to organic substance and salt, respectively),

$$\frac{\partial C}{\partial t} = [-\nabla \cdot (\mathbf{V}C) + \nabla^2 C] \text{ if } \phi = 0, \tag{3}$$

$$\frac{\partial C_{salt}}{\partial t} = [-\nabla \cdot (\mathbf{V}C_{salt}) + D_{salt}/D\nabla^2 C_{salt}] \text{ if } \phi = 0, \tag{4}$$

where $\mathbf{V}$ and p are the nondimensional velocity and pressure. The nondimensional form of the equations results from scal-

ing the lengths by a reference distance (L), the time by L^2/D; the initial values of the protein and precipitant agent (salt) are $C_{(0)}$ and $C_{salt(0)}$, respectively. Note that concentrations are not posed in nondimensional form ([g cm^{-3}]). The reference velocity and pressure are D/L and $\rho_S D^2/L^2$, respectively.

The solid phase (crystal) is assumed to be nondeforming and free of internal stress, while the multiphase region (region where phase change occurs) is viewed as a porous solid characterized by an isotropic pseudopermeability η by analogy with the enthalpy methods (see, e.g., Lappa [16,17]).

On the surface of the crystal ($|\nabla\phi| \neq 0, 0<\phi<1$), protein concentration satisfies the kinetic condition that in nondimensional form reads (n is the direction perpendicular to the crystal surface):

$$\left(\frac{1}{\rho_P - \rho_C C_i/\rho_S}\right)\frac{\partial C}{\partial n}\bigg|_i = \tilde{\lambda}(\sigma_i - 1 - \delta_0), \tag{5}$$

where $\tilde{\lambda}=\lambda L/D$, $\sigma=C/S$ is the degree of supersaturation, S is the solubility (its value is a function of the local concentration of the precipitant agent), ρ_P and ρ_c are the protein mass density and the total mass density in the crystal, ρ_S is the total density of the solution, δ_0 is the width of the supersaturation range in which no growth occurs (dead zone), and λ is the kinetic coefficient.

The phase field equation reads

$$\frac{\partial\phi}{\partial t} = 0, \quad \text{if } |\nabla\phi| = 0,$$

$$\frac{\partial\phi}{\partial t} = \frac{\tilde{\lambda}(\rho_P - \rho_C C/\rho_S)(C/S - 1 - \delta_0)\delta s}{\rho_P dv}, \quad \text{if } |\nabla\phi| \neq 0, \quad 0<\phi<1, \tag{6}$$

with C satisfying Eq. (5), where δs is the "reconstructed" portion of the crystal surface "bounded" by the frontier of the control volume (computational cell) located astride the crystal surface and dv is the volume of the computational cell (δs is provided by a PLIC technique [17]).

The code has been validated through comparison with the numerical results of Lin *et al.* [12]. The method is no longer discussed herein. For further details, the validation and the parallel implementation see Lappa [17] and Lappa [19], respectively.

B. Geometrical parameters and configuration under investigation

The growth of N seeds of lysozyme (see Table I for the properties of this molecule and the operating conditions for the simulations) is considered. Lysozyme has become over the years a very important "paradigm" model protein for fundamental research. Usually it is selected as the protein to crystallize because its solubility curve $S=S(C_{NaCl})$ is perfectly known and because of the current experience of organic crystal growers in producing gel reinforced crystals to be used as "seeds" for surface studies.

For the sake of simplicity (aim of the present paper is to elucidate convective and pattern-formation effects rather than the intrinsic surface-orientation-dependent growth mechanisms) the initial shape of the specimens is supposed to be quadrate (i.e., a horizontal layer of fluid confined between two parallel walls with a periodic array of evenly spaced square bodies in the interior) and the kinetic coefficient is supposed to be the same for the different sides of the crystal.

TABLE I. Properties and operating conditions.

D_{lys} [cm^2 s^{-1}]	10^{-6}
D_{NaCl} [cm^2 s^{-1}]	10^{-5}
ν [cm^2 s^{-1}]	8.63×10^{-3}
ρ_c [g cm^{-3}]	1.2
β_{lys} [g^{-1} cm^3]	0.3
β_{NaCl} [g^{-1} cm^3]	0.6
ρ_P [mg ml^{-1}]	820
λ [Å s^{-1}]	$\cong$10
δ_0 [−]	2
T [°C]	18
$C_{lys(0)}$ [g cm^{-3}]	6×10^{-2}
$C_{NaCl(0)}$ [g cm^{-3}]	2.5×10^{-2}
ℓ [mm]	1
L [mm]	10
PH	4.5

Relevant nondimensional geometrical parameters are the aspect ratio $A=H/L$ (see Fig. 1) of the reactor and the parameter $\kappa=\ell/d$ (ratio of the crystals size and related distance).

Following typical experimental procedures the seeds are supposed to be fixed (e.g., by glue) to the bottom of the reactor (see Fig. 1).

The present analysis focuses on the case of seeds located one away from the other at a distance of the order of the crystal size [$\kappa=O(1)$], changing their number and considering two different values of the aspect ratio of the reactor ($A=3$ and $A=6$).

The condition $\kappa=O(1)$ is investigated since (owing to the small size of the reactors used for morphological analyses) this is the typical situation occurring in this kind of studies. The number of seeds is changed in order to analyze the sensitivity of the overall system to this parameter. The dimen-

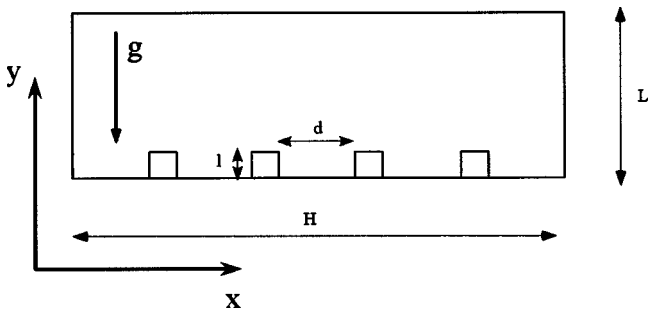

FIG. 1. Sketch of the growth reactor with the protein seeds and of the relative direction of the residual g.

sion of the reactor along x is doubled ($A=3 \rightarrow A=6$, retaining the same extension along y) in order to investigate the possible existence of regularities associated with transport process in a system with a large number of seeds—i.e., to discern if the domain can be split into a "central area" where the pattern is almost periodic and sides, close to the lateral no-slip walls (SW's), strongly affected by edge effects. Finally, the case with periodic lateral boundary conditions (PBC's) is considered to study the "idealistic" behavior in the case of infinite crystals at fixed values of the space parameter κ.

Growth is obtained from a supersaturated solution with $\sigma_{(0)} \cong 6$. With regard to this choice of initial conditions it should be pointed out that usually the protein concentration in the nutrient liquid is selected by organic crystal growers in order to favor growth and prevent new crystal formation (nucleation). For this reason the range of protein concentration and of supersaturation investigated is very limited. If protein concentration is too low, the seeds do not grow due to the "dead zone" [δ_0 in Eq. (1)]; if it is too high, new nuclei are formed and this phenomenon behaves as a disturbance for the growth and the study of the "seeds." For the case under investigation $\sigma_{(0)} \cong 6$ corresponds to a suitable and realistic condition.

The frontier of the domain is supposed to be impermeable to protein and salt (therefore the salt concentration is constant). According to the grid refinement study (not shown for the sake of brevity) a mesh 300×100 is used for the case $A=3$ and 600×100 for the case $A=6$.

III. RESULTS

As seeds grow from the solution, each crystal depletes the concentration of the growth units that are incorporated into the crystal lattice producing a concentration-depleted zone around it. In this region, the solute concentration changes continuously from the concentration at the crystal face to the concentration in the bulk of the solution. The concentration profile in the concentration-depleted zone varies with time as the crystal grows and is controlled by the balance between the flow of growth units towards the crystal face and the rate of incorporation of these growth units into the crystal lattice. The kinetics of incorporation at the crystal surface are linked to the bond configuration of the crystallographic structure as discussed in Sec. II A (for the present case of isotropic growth, the kinetics of incorporation are simply linked to the value of the kinetic coefficient and to the supersaturation level), while the flow towards the crystal face is highly dependent on the symmetry of the concentration pattern, which turns out to be crucial for the overall crystal growth process.

With regard to the latter aspect it is important to highlight how convection plays a critical role in determining the deformation of the concentration distribution around the growing crystals. The formation of halos due to the lowered solute concentration around growing seeds, in fact, has the effect of producing density gradients in these areas. These in turn (under the effects of gravity) result in the onset of convection.

These phenomena occur also during experiments in space. In fact, the residual gravity estimated on board the space shuttle and the International Space Station (ISS) is not zero, but typically of the order of 10^{-5} of Earth gravity. Therefore these effects have to be evaluated under microgravity conditions, in order to properly prepare and interpret the results of crystal growth experiments in space.

In addition to these arguments one must keep in mind that there is an effect related to the fact that, when many crystals grow in the same reactor, competition for growth occurs due to superposition and intersection of the related "depletion zones." The coupling between convective "pluming phenomena" and the overlapping of the depletion zones makes the concentration pattern very complex. It is worthwhile to highlight how in the presence of many growing crystals, the process is mainly controlled by these aspects.

A. Structure of the convective field

1. Lateral no-slip walls

First the attention is focused on the case of lateral no-slip walls (constant aspect ratio $A=3$ and two possible values of κ, and constant κ and two different values of the aspect ratio—i.e., $A=3$ and $A=6$), then the aforementioned condition with periodic side boundary conditions is taken into account.

For the case $A=3$, $g=10^{-4}\ g_0$, a flow field is driven by the density gradient around the growing crystals (see Figs. 2 and 3).

At the beginning [Figs. 2(a) and 3(a)] each crystal is characterized by its own rising solutal plume. In this early phase of the growth process—i.e., when depletion zones are separated—the growth dynamics of the different seeds can be regarded as independent. Two convective cells are generated around each crystal. After this initial transient behavior, however, the depletion zones for two growing consecutive seeds intersect and overlap [Figs. 2(b) and 3(b)]. At this stage mutual interference occurs. Crystals, in fact, absorb protein from "common" regions.

The delicate evolutionary equilibrium among crystal growth (absorption process), solution depletion phenomena, and competition among several seeds is coupled to significant and intriguing adjustments in the roll pattern inside the reactor.

A very complex multicellular structure is created above the interacting crystals. This convective field undergoes interesting subsequent transitions to different regimes as time passes. It is also worthwhile to stress how the major stages of this spatiotemporal evolution change according to the value of N ($N=5$, $\kappa=0.24$ in Fig. 2 and $N=6$, $\kappa=0.29$ in Fig. 3).

For the case $N=5$, at the beginning the mode of the multicellular field is $m=10$ [Fig. 2(a)] and five rising convective jets occur above the seeds (hereafter the crystals will be referred to as crystal i with $i=1 \rightarrow N$, respectively, starting from the left side of the reactor).

After 1.38×10^5 [s] [see Fig. 2(b)], the solutal plumes originated from crystals 1 and 2 merge giving rise to a single plume located at $x=H/4$. The same behavior holds for the seeds 4 and 5 since the system exhibits mirror symmetry with respect to the midsection $x=H/2$. For this reason the depleted lighter fluid is transported upwards by three solutal rising jets only. They are located approximately at $x=H/4$,

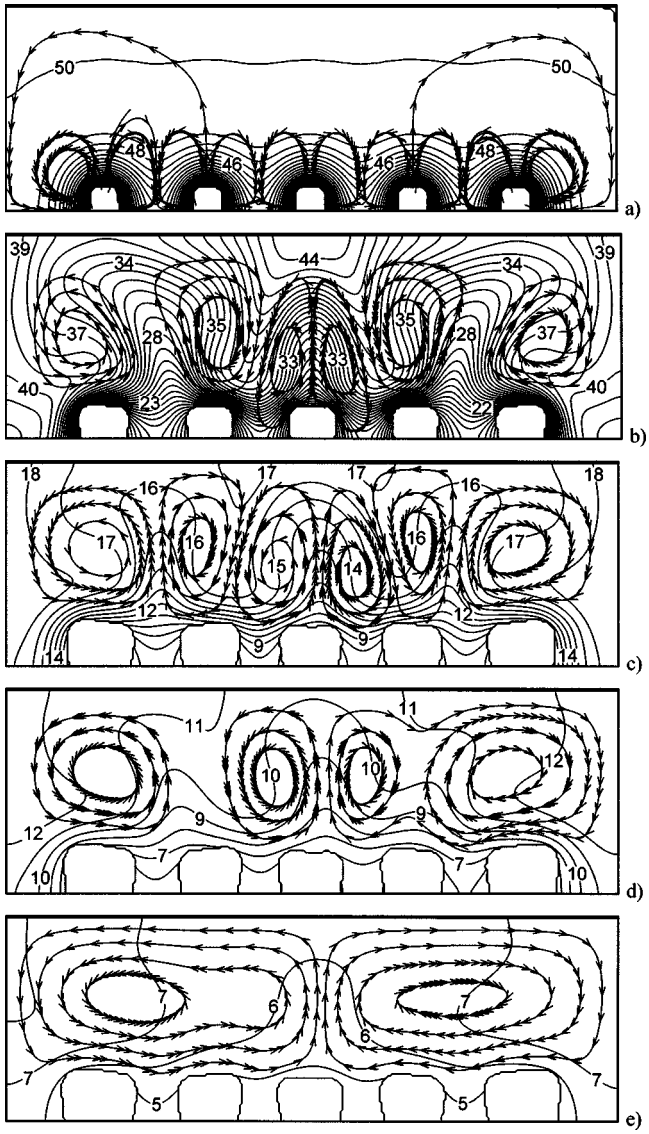

FIG. 2. Snapshots of growing crystals (SW, $A=3$, $N=5$), concentration distribution, and velocity field under microgravity conditions ($g=10^{-4}\ g_0$): (a) $t=1.38\times10^4$ [s], (b) $t=1.38\times10^5$ [s], (c) $t=3.59\times10^5$ [s], (d) $t=4.97\times10^5$ [s], (e) $t=7.18\times10^5$ [s] (level 1 $\rightarrow 2.8\times10^{-2}$ [g cm^{-3}], level $50\rightarrow 6\times10^{-2}$ [g cm^{-3}], $\Delta c=6.4\times10^{-4}$ [g cm^{-3}]).

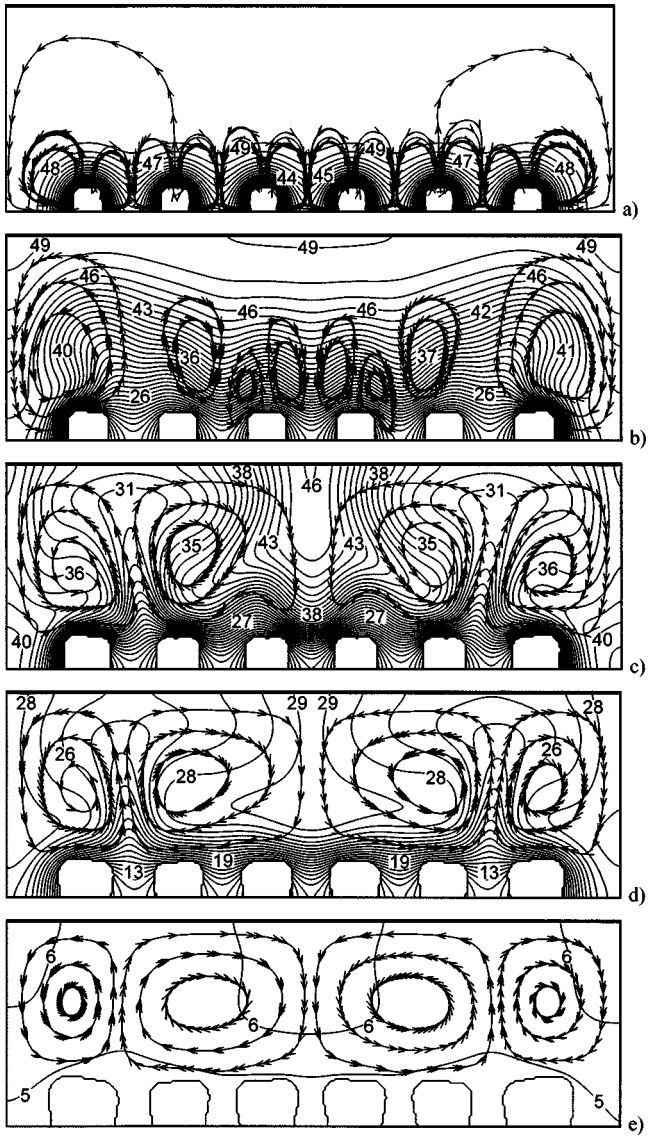

FIG. 3. Snapshots of growing crystals (SW, $A=3$, $N=6$), concentration distribution, and velocity field under microgravity conditions ($g=10^{-4}\ g_0$): (a) $t=1.0\times10^4$ [s], (b) $t=8.3\times10^4$ [s], (c) $t=1.35\times10^5$ [s], (d) $t=2.075\times10^5$ [s], (e) $t=8.3\times10^5$ [s] (level 1 $\rightarrow 2.8\times10^{-2}$ [g cm^{-3}], level $50\rightarrow 6\times10^{-2}$ [g cm^{-3}], $\Delta c=6.4\times10^{-4}$ [g cm^{-3}]).

$x=H/2$, and $x=3H/4$, respectively (instead of the five solutal plumes that characterize the system behavior in the early phase located at $x=iH/6$, $i=1\rightarrow5$). Correspondingly the initial number of rolls is reduced from 10 to 6. Two convective cells still exist above the central seed ($i=3$) whereas only two vortices characterize the right and left halves of the reactor with the core located approximately above the seeds 1,2 and 4,5, respectively. As time passes new regimes evolve which exhibit different number of rolls; the mode decreases to $m=4$ [$t\cong5\times10^5$ [s], Fig. 2(d)] and finally to $m=2$ [$t>5\times10^5$ [s], Fig. 2(e)] with only one vortex for each half of the reactor. The resulting two final convective cells have symmetric form, but rotate in the opposite direction; i.e., the flow is (approximately) symmetric by reflection about the midplane $x=H/2$.

For the case $N=6$ the roll-pattern formation and evolution are quite different. At the beginning the mode of the multicellular convective field is $m=12$ [Fig. 3(a)] and six rising plumes appear above the seeds ($i=1\rightarrow6$). For $t=8.3\times10^4$ [s] [see Fig. 3(b)], a large depletion zone surrounding all the crystals is formed and the mode is decreased to $m=8$; for $t=1.35\times10^5$ [s] [Fig. 3(c)] the depleted lighter fluid is transported upwards by two solutal rising jets only and the $m=8$ mode is taken over by a new regime with $m=4$. The surviving solutal plumes are located approximately at $x=H/4$ and $x=3H/4$, respectively, whereas the onset of pluming phenomena at $x=H/2$ is prevented. For $N=5$ around the midsection ($x=H/2$) the fluid is carried upwards, but for $N=6$ the opposite situation occurs. For $t>1.35\times10^5$ [s] [Figs.

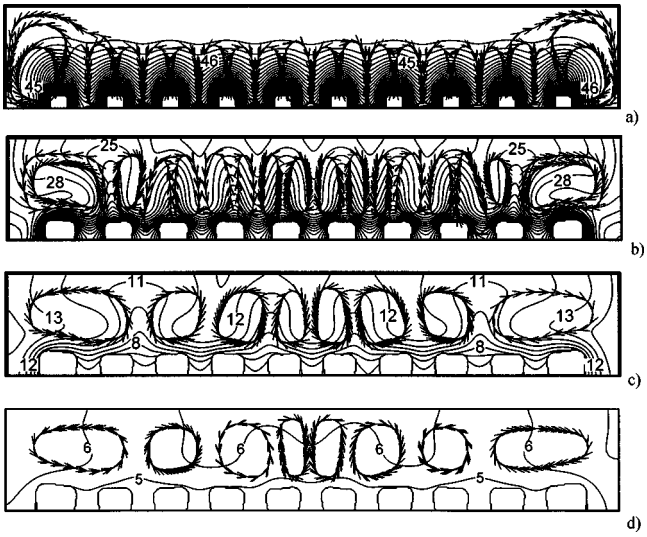

FIG. 4. Snapshots of growing crystals (SW, $A=6$, $N=10$), concentration distribution, and velocity field under microgravity conditions ($g=10^{-4}\,g_0$): (a) $t=4.6\times10^4$ [s], (b) $t=2.3\times10^5$ [s], (c) $t=4.83\times10^5$ [s], (d) $t=8.05\times10^5$ [s] (level $1\rightarrow2.8\times10^{-2}$ [g cm^{-3}], level $50\rightarrow6\times10^{-2}$ [g cm^{-3}], $\Delta c=6.4\times10^{-4}$ [g cm^{-3}]).

3(d) and 3(e)] the structure with four vortex cells seems to be quite stable without further transitions.

It is worthwhile to underline how the differences between the cases $N=5$ and $N=6$ could be used to explain in principle the scarce reproducibility that seems to characterize this kind of experiments (see also Ramachandran *et al.* [20]).

On the other side of the coin, the computations carried out increasing the extension of the protein reactor along x provide additional information about the effect of geometrical parameters, in particular with regard to possible existence of a "core zone."

Along these lines, Fig. 4(a) shows that for the case $A=6$, $N=10$ at the beginning each crystal is characterized by its own rising solutal plume with the exception of the crystals located at the extremities. After a transient time four solutal jets are created above the seeds [Fig. 4(c) and the mode is $m=8$. This situation seems to be quite stable [see Fig. 4(d)].

As expected, with the exception of the two crystals at the edges, an interesting spatial periodic behavior arises along x in this case. The seeds seem to "work" in groups of two. Rising solutal jets are created above the couples (2,3) (4,5) (6,7) (8,9), and descending jets occur above the couples (3,4) (5,6) (7,8). Therefore a certain degree of periodicity in space can be highlighted with a central zone affected by a somewhat "repetitive" behavior.

This trend is confirmed by the simulations carried out for $A=6$ and $N=12$ (not shown). Accordingly, some general rules can be introduced for the case with no-slip lateral walls. If the aspect ratio is sufficiently large and $\kappa=O(1)$, in fact the final mode can be roughly computed as $m=(N-2)$ and the number of rising solutal jets as $(N-2)/2$.

Hereafter, the results pertaining to the PBC case are elucidated.

2. Periodic lateral boundary conditions

These simulations, specially conceived to allow for lateral freedom, on the one hand give indirect evidence of the fact

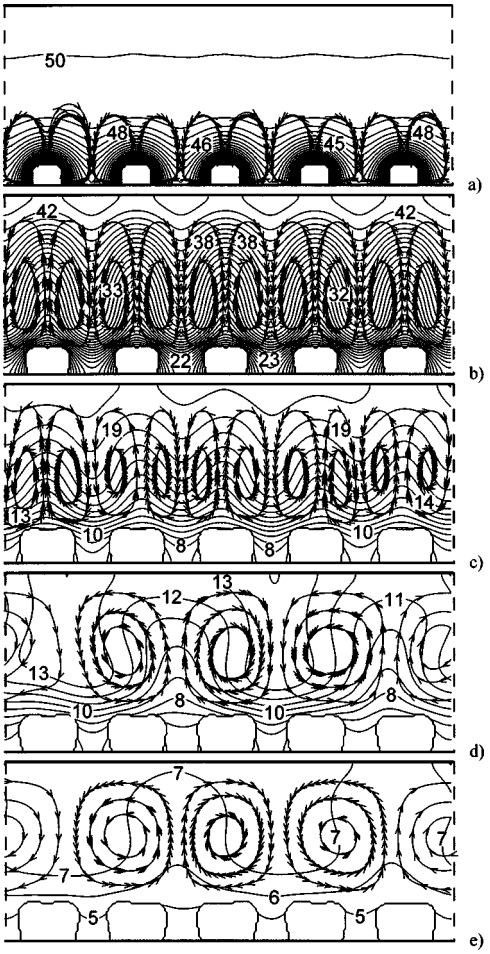

FIG. 5. Snapshots of growing crystals (PBC, $\kappa=0.24$, $N=5$), concentration distribution, and velocity field under microgravity conditions ($g=10{-}4\ g_0$): (a) $t=1.38\times10^4$ [s], (b) $t=1.38\times10^5$ [s], (c) $t=3.59\times10^5$ [s], (d) $t=4.97\times10^5$ [s], (e) $t=7.18\times10^5$ [s] (level $1\rightarrow2.8\times10^{-2}$ [g cm^{-3}], level $50\rightarrow6\times10^{-2}$ [g cm^{-3}], $\Delta c=6.4\times10^{-4}$ [g cm^{-3}]).

that the sidewalls can still have a significant influence on the resulting velocity and solutal fields even if $A\gg1$ (e.g., $A=6$; see the last part of this section for further details); on the other hand, they provide a variety of interesting insights into the "extreme" behavior, which the system tends to, when the number of interacting crystals is increased to infinite ($N\rightarrow\infty$) at fixed values of the interspace parameter κ (i.e., infinite layer of liquid with evenly spaced seeds in the interior).

As a first step, comparison between the computations for $\kappa=0.24$ and $N=5$ (PBC, shown in Fig. 5) and those for $A=3$ (SW) and same value of κ (Fig. 2) highlights that in the absence of side solid constraints, the delicate evolutionary equilibrium among the rolls is featured by a different time history.

The initial multicellular pattern with a clockwise and a counterclockwise rotating cell around (above) each seed, in fact, tends to be more stable (compare, e.g., frames 2(a)–2(c) and 5(a)–5(c)); this means that, when PBC's are considered, the coalescence process of adjacent vortices, observed in the SW case, is postponed in time. The differences, however, are not limited to the temporal sequence of transitions to differ-

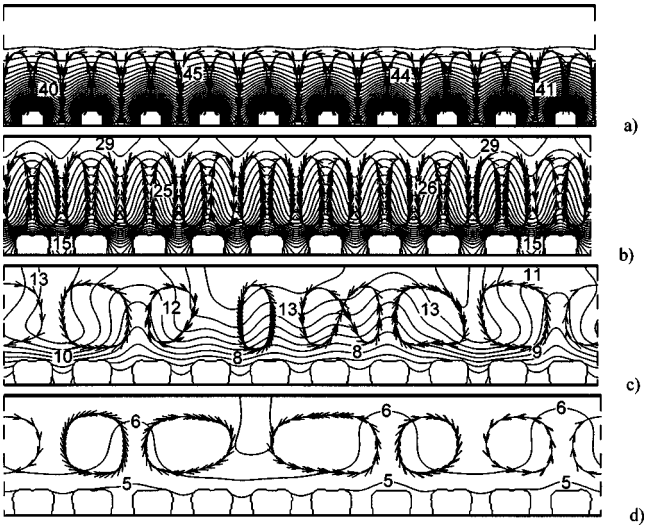

FIG. 6. Snapshots of growing crystals (PBC, $\kappa=0.24$, $N=10$), concentration distribution, and velocity field under microgravity conditions ($g=10^{-4}\ g_0$): (a) $t=4.6\times10^4$ [s], (b) $t=2.3\times10^5$ [s], (c) $t=4.83\times10^5$ [s], (d) $t=8.05\times10^5$ [s] (level $1\rightarrow2.8\times10^{-2}$ [g cm^{-3}], level $50\rightarrow6\times10^{-2}$ [g cm^{-3}], $\Delta c=6.4\times10^{-4}$ [g cm^{-3}]).

ent regimes. The roll-pattern formation and evolution lead to a final state with four major rolls [Fig. 5(e); they are two in the SW case; see Fig. 2(e)].

In the light of these arguments, the absence of lateral solid constraints can be thought of as altering the mode selection process and the pattern symmetries. This result is not unexpected (see, e.g., the theoretical arguments in the next section). For an even more deep perspective into this topic, however, it is necessary to stress that the periodic domain length (H_p) used for the simulations should be regarded as an additional sensitive parameter for such selection mechanisms.

Special care must be devoted to this aspect for obtaining a periodic-length-independent solution. As previously explained, the rolls adjustment process occurs by coalescence of adjacent cells and possible ensuing expansion and contraction of the resulting vortex. However, when PBC's are employed, the pattern is constrained to be periodic over the chosen H_p; i.e., the ratio of the periodic width to the wavelength is forced to be an integer number.

If the most dangerous (hereafter referred to as "natural") disturbances involve concentration and velocity fields with a periodic extent that is larger than the chosen H_p (i.e., they have a wavelength that is not commensurable to H_p), the system will select disturbances that are not natural; i.e., a not suitable periodic length may force the system to select a small wavelength and therefore to select a different symmetry of the disturbances (e.g., an even mode instead of an odd mode).

Additional simulations carried out with a doubled periodic horizontal width in order to remove the restriction limiting the possible disturbances (by allowing the convection rolls to continuously coalesce, expand, or compress over a larger distance; see Fig. 6) show, in fact, that further adjustment occurs when the allowed degree of freedom along the horizontal direction is increased—i.e., a larger wavelength is selected; for $\kappa=0.24$ and $N=10$, the final multicellular state involves six counterotating vortices and three ascending plumes.

FIG. 7. (PBC, $\kappa=0.24$, $N=20$), crystal distribution and velocity field under microgravity conditions ($g=10^{-4}\ g_0$): $t=8.05\times10^5$ [s].

At this stage, it is worthwhile to shed some light on the physical mechanisms by which m is selected.

Discrete wave numbers of disturbances are selected out of the full spectrum of disturbances because the multicellular structure is closed in a special zone geometry. As anticipated, the selection rule is given by the constraint that the wavelength must be an aliquot of the periodic horizontal extent; however, the geometrical constraints represented by the presence of top and bottom boundaries also play a role is such mechanisms.

The simulations in Figs. 5 and 6 show that the final size of the crystals along y is about twice the initial seed size "ℓ." Therefore the space occupied by the rolls along y is about $(L-2\ell)$; since the size of each convective cell along x tends to be approximately equal to its extension along y, the m rolls cover a distance $m(L-2\ell)$. Obviously, such a distance must be equal to the periodic width, and since the periodic horizontal extension can be also computed as $N(\ell+d)$, this leads to

$$m(L-2\ell)=N(\ell+d), \tag{7a}$$

which, taking into account $\ell/d=0.24$ ($d\cong4\ell$) and $\ell=L/10$ (see Table I), reads

$$8m=5N. \tag{7b}$$

Equations (7) provide an analytical relationship between the mode and the number of crystals (evenly spaced over the periodic length) supported by precise theoretical arguments. For increasing values of N, Eq. (7b) gives

$$N=5\rightarrow m\cong3, \tag{8a}$$

$$N=10\rightarrow m\cong6, \tag{8b}$$

$$N=20\rightarrow m\cong12. \tag{8c}$$

Equation (8a) does not agree with the numerical results ($m=4$ in Figs. 5), but the agreement holds for $N=10$ as shown in Figs. 6. This proves (as speculated in the foregoing discussion) that the results in Fig. 5 do not represent a periodic-length-independent solution. Additional theoretical relevance to these aspects can be simply obtained by further doubling the periodic width along x. The mode number for the corresponding results in Fig. 7 is $m=12$ as predicted by Eq. (8c). This finally demonstrates that convergence in the disturbances selection mechanism is achieved for sufficiently large horizontal periodic distance (for the considered case it is $2H_p^5$ where H_p^5 is the periodic length used for the simulation in Fig. 5).

In practice, numerical simulations of the conditions corresponding to Eq. (8a) are not relevant since it is obvious that odd modes (e.g., $m=3$) cannot be captured by numerical simulations with PBC's (with such conditions there must be the same number of clockwise- and counterclockwise-oriented vortex cells). The number of rolls in a PBC system with a moderate extension that does not match a multiple of the natural wavelength of the instability is not "physical." The convective rolls are more regular and their number scales according to Eq. (7b) when the width is closer to a multiple of the natural wavelength (Figs. 6 and 7).

Among other things, as anticipated, when compared to the corresponding case with solid side walls, these results also elucidate [compare Figs. 4(d) and 6(d)] that the aforementioned existence, for sufficiently large but "finite" values of the aspect ratio, of a core zone with periodic convection and very small wavelength must still be regarded as an effect of the lateral geometrical constraints.

B. Comparison with the classical Rayleigh-Bènard system: Analogies and differences

It is noteworthy how, from a fluid-dynamic point of view, the problem under investigation exhibits quite an interesting theoretical kinship with the Rayleigh-Bènard (RB) system in which convection is induced in a horizontal fluid layer by uniform heating from below. Therefore, it is opportune to open a short discussion about the related analogies and differences. Such a critical comparison can be regarded as an additional theoretical artifice by which additional insights into the physics and the results described in the earlier section can be obtained.

Rayleigh–Bènard convection is a canonical example of a pattern-forming system. A fascinating question is raised by the pattern selection process upon which a convection layer evolves through time to a final state. Wave number selection has been well studied with many different mechanisms now well characterized.

Most of the initial studies considered infinite systems—i.e., the stability of the quiescent state of nonconfined fluid layers heated from below. It was found that such layers undergo instability to couples of counterotating convective rolls with aspect ratio (ratio of the couple width to the depth of the layer) $A_c \cong 2$ (see, e.g., Drazin and Reid [21]).

Currently, however, it is well known that if systems confined laterally by rigid sidewalls are considered, even in containers of large horizontal dimensions, the lateral walls can have a significant influence on the flow pattern that develops when the Rayleigh number exceeds its critical value. Thus results for the corresponding infinite layer cannot, in general, be used to make predictions about either the detailed structure or the stability of the roll pattern in practical situations.

It has been clearly illustrated by many investigators, in fact, that there are several modes of the most dangerous perturbation that replace each other when the aspect ratio A (ratio of the width and of the height of the finite layer) is varied (see, e.g., Gelfgat [22]). Within this context it should also be mentioned that the increase of the aspect ratio A generally results in the increase of the number of two-dimensional rolls within the finite-size rectangular container. This is in agreement with the present SW results.

Several studies have also elucidated that in large convection layers (where the lateral extent is much larger than the depth) for fixed values of A and Rayleigh numbers in the range $\mathrm{Ra}=\mathrm{Ra}_\infty+O(2/A)$ where Ra_∞ is the critical Rayleigh number for the corresponding infinite layer, there exists a class of finite-amplitude steady-state two-dimensional "phase-winding" solutions that correspond physically to the possibility of an adjustment in the number of rolls in the container (by coalescence mechanisms similar from a qualitative point of view to those described in the earlier paragraph) as the local value of Rayleigh number is varied [23].

It is also known [24] that in RB periodic convection layers the wavelength of convection rolls also changes in other simpler situations where the mode selection process appears to be governed by a two-dimensional process involving parallel convection rolls undergoing a wave number adjustment by a simple roll expansion (the so-called "roll relaxation" by which the convection rolls increase in wavelength to values larger than the value at threshold). Evidence of such a two-dimensional relaxation mechanism has been found in both experiments and numerics.

In light of all these arguments, the Rayleigh-Bènard problem has, therefore, solid theoretical bases; several experimental and numerical works have been performed in order to confirm the theoretical assumptions. Nonlinear effects and geometrical constraints are all essential ingredients of this type of flow. According to the aforementioned "analogy," these features may provide a somewhat relevant theoretical background to explain the trends observed for the present case of a liquid layer with crystals on the bottom; among them are the observed change in wave number as a function of the aspect ratio when SW conditions are considered, the roll-adjustment process, and the observed notable differences between the SW and PBC cases.

Despite the macroscopic qualitative similarities, however, the dynamics and mechanisms underlying the evolution of the present system are quite different.

In the case of uniformly heated layers the driving force for the onset of convection is the lighter fluid on the bottom of the container, this "force" being replaced by the presence of a discrete distribution of sinks of solute for the case of a discrete layer of growing macromolecular crystals (the incorporation of protein is the source of lighter fluid at the crystals surface). However, there is no doubt that the geometries that arise in protein crystal growth applications are more complicated than a simple horizontal layer of convecting fluid. For such a case the "heating" is not uniform. The depletion zones do not exhibit uniform behavior. Moreover, during the initial stages of convection fluid motion also arises along the vertical boundaries of the crystals (this effect is not present in the classical Rayleigh-Bènard system; within the framework of the proposed analogy, it would correspond to a "heating-from-the-side" thermal condition).

For many interacting crystals, the adjustment in the number of rolls occurs as a consequence of the coalescence mechanism of the depletion zones that merge as time passes (the samples grow and the related "halos" become larger and overlap); there is an undeniable effect of the number of crys-

tals and their distribution. Along these lines, for instance, it is worth pointing out that an initial nonuniform distribution of the seeds could deeply affect the initial interaction mode. In that case in fact the initial interaction would occur between the seeds with small distance.

Other factors influencing the roll-adjustment process are the effective driving force acting in the liquid (the instantaneous Rayleigh number decreases in time owing to the protein absorption process) and the space occupied by the crystals that continuously increases (this behavior is responsible for the confinement of the overall convective structure to the upper part of the reactor). Therefore, for the growth of many aligned evenly spaced macromolecular seeds, after the early stages (with an alternating array of clockwise and counterclockwise rotating cells, each couple being located around an internal seed), the process by which the instantaneous mode is selected is very complicated (possibly involving the effects of multiple incommensurate selection mechanisms). There are at least five independent parameters influencing the aforementioned evolution of the multicellular structure: i.e., the aspect ratio of the protein reactor and/or the type of lateral boundary conditions, the time evolution of the phenomenon of absorption of protein (this would correspond to a quasisteady variation of the Rayleigh number for the case of the layer of fluid heated from below), the coalescence process of the depletion zones originated from different seeds, and finally (as previously highlighted) the number of interacting protein crystals and the growth process itself (which leads to a confinement of the roll pattern to the top of the reactor due to the increasing size of the underlying crystals).

In practice, such a system "ideally" tends to the behavior of the classical infinite RB problem only when PBC conditions are considered and, in particular, only during the very final stages of convection. For a very reduced crystal interspacing (final stage of the growth process), in fact, the convective rolls do present the most unstable wavelength typical of the classical Rayleigh-Bènard instability—i.e., the ratio of the width of a couple of vortices to the depth of the layer $\cong 2$ [i.e., the aspect ratio of each roll $\cong 1$ as also discussed in Sec. III A 2 in the derivation of Eqs. (7)]. This occurs since the process is no longer affected by changes in the geometry of the crystals, the rate of change in time of the concentration gradient between the seeds, and the liquid is so small that the Rayleigh number can be regarded as constant, and the isocontour lines pertaining to the depletion zones are almost horizontal and uniform (the individual crystals seem to behave as one).

C. Growth rate distribution and morphological instabilities

The earlier discussion is quite a comprehensive analysis of the fluid dynamics associated with the growth of the seeds and may provide interesting information and data for fundamental fluid-dynamic research and for investigation of nonlinear behaviors. The present paragraph deals with the growth process itself.

The cases with an infinite number of seeds (PBC's) and/or very high aspect ratio are not treated herein since they are not of practical interest. As previously discussed, in fact, a very large number of crystals are grown by organic crystal growers using gellified configurations where convective effects cannot occur. Therefore, hereafter the analysis is limited to the SW case and $A=3$.

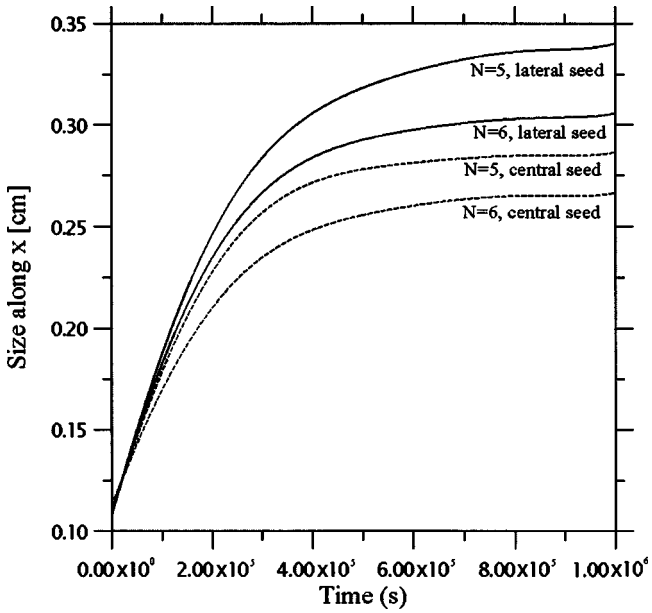

FIG. 8. Average size (along x) of the growing seeds versus time (SW, $A=3$).

Before starting to deal with the "local" detailed analysis of each crystal according to its position some common features can be pointed out.

Figures 2 and 3 show that the "depth" of the face protuberances is proportional to the size of the crystals (competition for growth in the intermediate regions and corner effects are responsible for the tooth shape of the crystals). Moreover, the increase of volume is more pronounced for the crystals at the extremities of the reactor ($i=1$ and $i=5$ for $N=5$, $i=1$ and $i=6$ for $N=6$, $i=1$ and $i=10$ for $N=10$) than for the central crystals ($i=3$ for $N=5$, $i=3$ and $i=4$ for $N=6$). This trend is confirmed by Fig. 8 where the size of the seeds along x is plotted as a function of time. This plot also highlights that the increase of volume is less pronounced in the case $N=6$ with respect to $N=5$. This apparent "lack" of solid mass of course follows from the presence of a higher number of crystals simultaneously absorbing protein from the liquid phase in the case $N=6$ (i.e., for a fixed initial amount of protein available in liquid phase, the final size of the crystals decreases as their number increases).

Possible explanations of the above trends can be outlined on the basis of the local growth rate distributions plotted in Figs. 9 and 10.

In agreement with previous results [16,17] these figures show that corners and edges of the crystals are more readily supplied with solute than the center of sides (this is responsible for the morphological instability and the presence of a macroscopic depression around the center of the faces shown in Figs. 2 and 3).

As previously discussed, incorporation of the solute into the crystal causes a local depletion in concentration and a

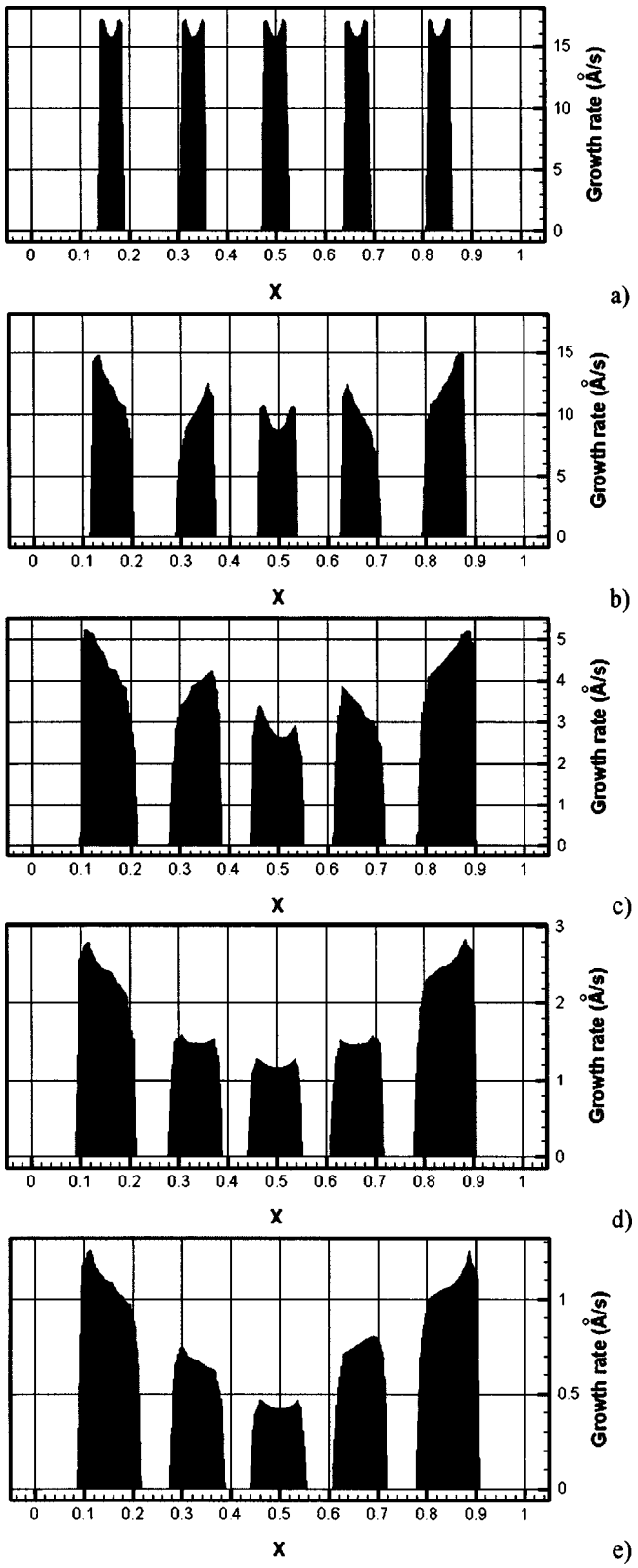

FIG. 9. Snapshots of growth rate distribution, SW, $A=3$, $N=5$: (a) $t=1.38\times10^4$ [s], (b) $t=1.38\times10^5$ [s], (c) $t=3.59\times10^5$ [s], (d) $t=4.97\times10^5$ [s], (e) $t=7.18\times10^5$ [s].

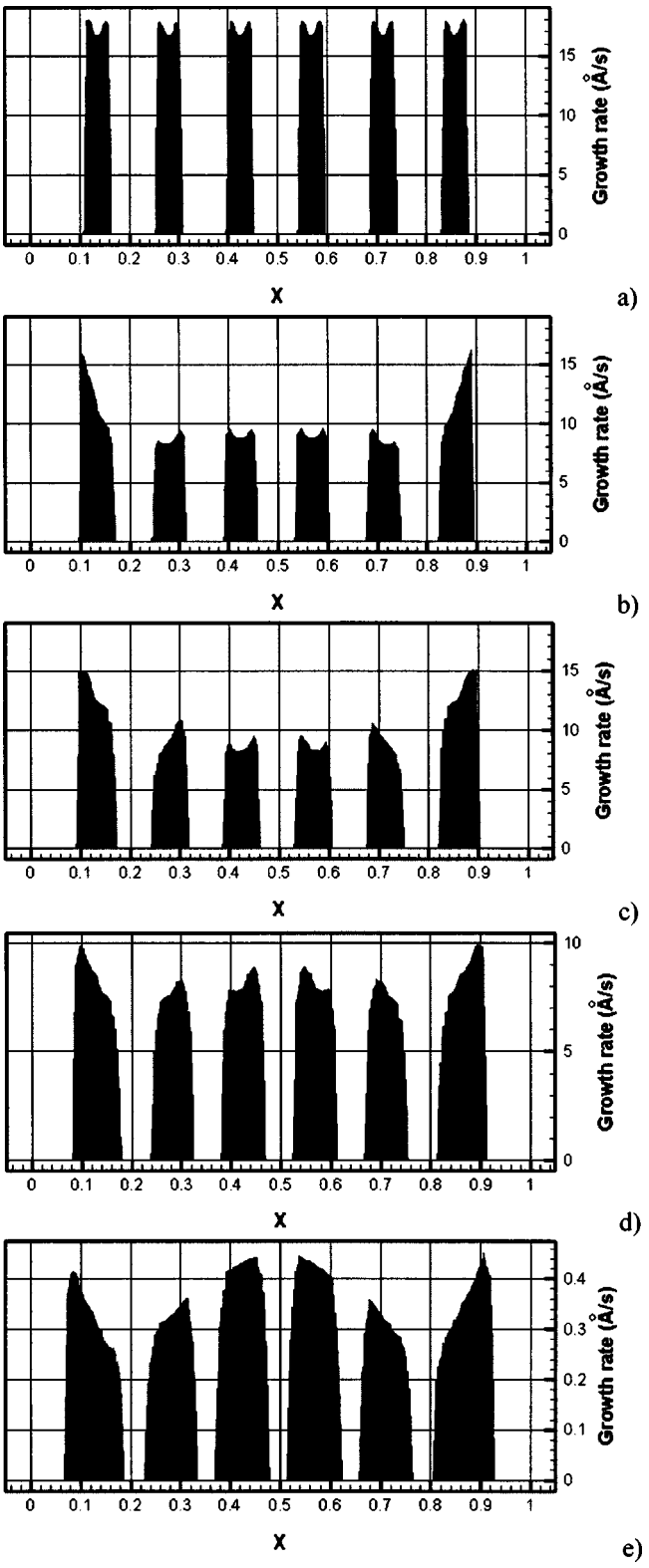

FIG. 10. Snapshots of growth rate distribution, SW, $A=3$, $N=6$: (a) $t=1.0\times10^4$ [s], (b) $t=8.3\times10^4$ [s], (c) $t=1.35\times10^5$ [s], (d) $t=2.075\times10^5$ [s], (e) $t=8.3\times10^5$ [s].

solutal concentration gradient to form between the bulk solution and the growth interface. As expected, the growth rate is always lower at the center than at the corners where the convective flows (and the associated shear stresses) are the strongest, and hence, the interfacial concentration gradients the steepest.

Figures 9 and 10 also allow to point out that the difference in gradient steepness (i.e., local growth rate) between the face corner and face center increases as time passes; this explains why the "depth" of the face depressions is proportional to the volume of the samples. Moreover, the convection effects tend to increase the local growth rates for the crystals at the extremities. This trend finally provides a justification for the behaviors shown in Fig. 8.

Despite the macroscopic analogies and similarities pointed out above, however, each crystal exhibits different morphological evolution and different growth history according to its position within the reactor and according to the value of N.

For instance, in the case $N=5$ the final "ridge" (slope of the upper side) of the crystals with $i \neq 3$ is inclined with respect to the direction of the residual g [on the contrary for $i=3$ the ridge is almost flat and horizontal, Fig. 2(e)]. For $i=1$ and $i=5$ the ridge is inclined inwardly, and vice versa for $i=2$ and $i=4$ it is inclined outwardly. For the case $N=6$, the ridge is inclined inwardly for $i=1$ and $i=6$ and outwardly for $i=2,3,4,5$ [Fig. 3(e)]. "Edge effects" are also very evident in Fig. 4(d).

In practice the characters of the final samples change depending on the local fluid-dynamic conditions under which they are operated. In addition to the effect associated with the corners more readily supplied with solute, there is an effect due to the local convective pattern around the crystal. The cross-comparison frame by frame of Figs. 2 and 9 for the case $N=5$ (3 and 10 for the case $N=6$) in particular elucidates that the convection effect results in higher local growth rates near the surface where the flow is directed downwards and lower local growth rates near the surface where the flow is carried upwards (as depicted in detail in Sec. III A 1, if the number of seeds is not sufficiently large these fluid-dynamic conditions in turn change in time and exhibit a different spatial evolution according to the number of interacting crystals simultaneously growing in the protein reactor).

It is very important to point out how the correspondence elucidated above between surface growth rates and roll pattern evolution is an indirect evidence of the fact that for the case under investigation, mass transport in the bulk and surface attachment kinetics are competitive as rate-limiting steps for growth (in the case of phenomena strictly governed by the kinetic barrier in fact the effect of convection on the overall growth process is almost negligible).

IV. CONCLUSIONS

The different complex scenarios that arise in a growth reactor (accommodating many protein seeds) in terms of detailed structure of the convective field and distribution of the local growth rates have been investigated for the first time in the framework of a recently introduced volume tracking method. This multiphase methodology has been used to address the geometric complexity introduced by the internal seeds and their growth process.

The face growth rates have been found to depend on the time-dependent multicellular structure of the velocity field and to be nonuniform across the crystal face (growth rate always lower at the center than at the corner).

The prominent features of this evolution exhibit large sensitivity on the number of crystals simultaneously growing in the protein reactor if this number is not sufficiently large (this case corresponds to typical experiments carried out by organic crystal growers interested in studying morphological and kinetic details). It, in fact, plays a crucial role in determining the mode of the convective field (i.e., the number of vortex cells), the number and positions of rising solutal jets, and the related time evolution.

On the contrary some general rules can be introduced to characterize the system behavior if the number of seeds and the aspect ratio are large. The direction of the jets in this case in fact results modulated in space with an evenly spaced alternation of rising and descending jets. This behavior holds for a "central zone" of the reactor not affected by edge effects. Additional simulations carried out using periodic boundary conditions show, however, that the existence of the aforementioned core region is made possible by the effect exerted by the no-slip side walls that lead to small values of the internal wavelength. In the case of periodic domain, in fact, the delicate evolutionary equilibrium among the rolls is featured by a different time history and the final wavelength is larger. The simulations also show that the relaxation of convection rolls in the periodic layer depends on the length of the computational domain. Hence, the choice of this width is a very delicate aspect of the simulation strategy when trying to capture the behavior of a system with infinite extent.

The results are heretofore unseen and elucidate how protein seeds can exhibit different shape evolution and different growth history according to the position within the reactor—i.e., according to the "local" fluid-dynamic conditions.

The morphological evolution of the seeds has proven to be strictly coupled to the sequence of transitions that characterize the fluid motion. The growth of the crystals in turn influences the stages of evolution of the velocity field being responsible for the confinement of the overall convective structure to the upper part of the reactor. Possible theoretical kinship with the case of the Marangoni-Bènard problem has been discussed, pointing out analogies and differences. It is not possible to predict *a priori* the mode that will appear under the assigned conditions through analogy with the canonical Rayleigh-Bènard problem because the present phenomena are influenced by many parameters, incommensurate wavelength selection mechanisms, and the "history" of the flow.

This study represents a first (and quite exhaustive) attempt to discern the cause and effect relationships underlying the complexity of growth carried out in the presence of many interacting crystals. Determining the related growth laws is central for discerning how (fluid-dynamic) environment conditions affect macromolecular growth. The mutual interaction between the onset of morphological instabilities (depressions and/or protuberances in the shape of the crystal)

occurring in "growing" solid walls and the fluid motion (multicellular structure of the flow, solutal jets, shear stress distribution, etc.) provides rich information to be used in the framework of macromolecular crystallization.

The present work introduces a common source made available for fluid-dynamic researchers (the paper provides interesting information about the mechanics of the *fluid motion per se* and the dynamics of an intriguing and still unexplored pattern forming dynamical system) and for organic crystal growers (the paper elucidates the morphological evolution of the crystals).

ACKNOWLEDGMENTS

This work has been supported by ASI (Italian Space Agency) and ESA (European Space Agency). For additional material, color figures and animations see http://staff.marscenter.it/lappa and http://utenti.lycos.it/MarcelloLappa.

[1] P. G. Vekilov and A. A. Chernov, *The Physics of Protein Crystallization*, *Solid State Physics*, Vol. 57, edited by H. Ehrenreich and F. Spaepen (Academic Press, Amsterdam, 2002), pp. 1–147.
[2] A. McPherson, Eur. J. Biochem. **189**, 1 (1990).
[3] F. Otálora and J. M. Garcìa-Ruiz, J. Cryst. Growth **182**, 141 (1997).
[4] F. Otálora, M. L. Novella, J. A. Gavira, B. R. Thomas, and J. M. Garcìa-Ruiz, Acta Crystallogr., Sect. D: Biol. Crystallogr. **57**, 412 (2001).
[5] F. Otálora, J. M. Garcìa-Ruiz, L. Carotenuto, D. Castagnolo, M. L. Novella, and A. A. Chernov, Acta Crystallogr., Sect. D: Biol. Crystallogr. **58**, 1681 (2002).
[6] C. P. Lee and A. A. Chernov, J. Cryst. Growth **240**, 531 (2002).
[7] C. Piccolo, M. Lappa, A. Tortora, and L. Carotenuto, Physica A **314**, 636 (2002).
[8] L. Carotenuto, C. Piccolo, D. Castagnolo, M. Lappa, and J. M. Garcìa-Ruiz, Acta Crystallogr., Sect. D: Biol. Crystallogr. **58**, 1628 (2002).
[9] M. Lappa, C. Piccolo, and L. Carotenuto, J. Cryst. Growth **254**, 469 (2003).
[10] M. Lappa, D. Castagnolo, and L. Carotenuto, Physica A **314**, 623 (2002).
[11] M. Lappa and D. Castagnolo, Numer. Heat Transfer, Part B **43**, 373 (2003).
[12] H. Lin, F. Rosenberger, J. I. D. Alexander, and A. Nadarajah, J. Cryst. Growth **151**, 153 (1995).
[13] D. S. Noh, Y. Koh, and I. S. Kang, J. Cryst. Growth **183**, 427 (1998).
[14] W. J. Rider and D. B. Kothe, J. Comput. Phys. **141**, 112 (1998).
[15] Y. T. Kim, N. Goldenfeld, and J. Dantzig, Phys. Rev. E **62**, 2471 (2000).
[16] M. Lappa, J. Theor. Biol. **224**, 225 (2003).
[17] M. Lappa, J. Comput. Phys. **191**, 97 (2003).
[18] M. Lappa, Phys. Fluids **15**, 1046 (2003). This article has been also selected by the American Physical Society for the 15 March 2003 issue of the Virtual Journal of Biological Physics Research (Volume 5, Issue 6).
[19] M. Lappa, *Fluids, Materials and Microgravity: Numerical Techniques and Insights into the Physics* (Elsevier Science, Oxford, 2004), pp. 1–523.
[20] N. Ramachandran, Ch. R. Baugher, and R. J. Naumann, Microgravity Sci. Technol. **8**, 170 (1995).
[21] P. G. Drazin and W. H. Reid, *Hydrodynamic Stability* (Cambridge University Press, Cambridge, UK, 1981).
[22] A. Yu. Gelfgat, J. Comput. Phys. **156**, 300 (1999).
[23] P. G. Daniels, J. Fluid Mech. **143**, 125 (1984).
[24] M. R. Paul and I. Catton, Phys. Fluids **16**, 1262 (2004).